Integrated acoustic and magnetic separation in microfluidic channels

Jonathan D. Adams,[1] Patrick Thévoz,[2,3] Henrik Bruus,[4] and H. Tom Soh[2,5,a)]
[1]*Department of Physics, University of California–Santa Barbara, Santa Barbara, California 93106, USA*
[2]*Department of Mechanical Engineering, University of California–Santa Barbara, Santa Barbara, California 93106, USA*
[3]*Microsystems for Space Technologies Laboratory, Ecole Polytechnique Fédérale de Lausanne (EPFL), CH-2002 Neuchatel, Switzerland*
[4]*Department of Micro- and Nanotechnology, Technical University of Denmark, DK-2800 Lyngby, Denmark*
[5]*Department of Materials, University of California–Santa Barbara, Santa Barbara, California 93106, USA*

(Received 26 August 2009; accepted 31 October 2009; published online 21 December 2009)

With a growing number of cell-based biotechnological applications, there is a need for particle separation systems capable of multiparameter separations at high purity and throughput, beyond what is presently offered by traditional methods including fluorescence activated cell sorting and column-based magnetic separation. Toward this aim, we report on the integration of microfluidic acoustic and magnetic separation in a monolithic device for multiparameter particle separation. Using our device, we demonstrate high-purity separation of a multicomponent particle mixture at a throughput of up to 10^8 particles/hr. © *2009 American Institute of Physics*. [doi:10.1063/1.3275577]

As cell-based biotechnological applications continue to increase in prominence,[1,2] there is an urgent demand for cell sorting approaches that offer consistently high purity, recovery, and throughput. Fluorescence activated cell sorting[3] allows multiparameter separation but is limited by low throughput[4] potential damage to cells[5] and cost. In contrast, column-based magnetic separation[6,7] enables higher throughput but only allows for single-parameter separation. Continuous flow separation approaches based on microfluidics technology present a compelling alternative; microfabrication techniques offer precise control and integration of multiple separation forces in a noninteracting manner, thereby enabling high-performance, multiparameter cell sorting in disposable devices.[8–10]

We report here on the integration of acoustic and magnetic separation forces in a monolithic device, demonstrating high-purity, multiparameter particle separation in a continuous flow manner. This pairing of forces is especially useful because it combines label-free separation (acoustophoresis)[11] with molecular label-based separation (magnetophoresis).[12–14] In addition, neither separation force is significantly affected by pH, salinity, temperature, and other characteristics of the suspension medium, such that the method can be used for a wide range of cell types and samples.

The integrated acoustic-magnetic separation (IAMS) device has two inputs and three outputs, and integrates the acoustic and magnetic separation in a serial manner. A sample containing a mixture of acoustic target, magnetic target, and nontarget particles is injected into the sample injet and maintained close to the channel wall by a parallel buffer stream (Fig. 1). All particles then pass through an acoustic separation region, where the nontarget particles are separated from the sample via acoustophoresis and elute into the waste outlet (Fig. 1, inset left). Acoustic and magnetic target particles are subsequently separated by a series of microfabricated ferromagnetic structures, which selectively deflect the magnetic target particles into a different flow-stream (Fig. 1, inset right). In this way, particles are separated to elute through three separate outlets. The IAMS device (Fig. 2) is fabricated using standard microfabrication techniques.[15] The device is placed over an inverted microscope and monitored during separation. Outlet fractions are independently collected and the purities are analyzed via flow cytometry [Fig. 2(b)].

Quantitatively, the acoustic primary radiation force exerted on a particle surrounded by fluid in our channel geometry is given by[16]

$$\langle \mathbf{F}_{\mathrm{ac}} \rangle = \langle E \rangle \frac{\omega V}{c_o} \left[\frac{5\alpha - 2}{2\alpha + 1} - \frac{1}{\alpha \beta^2} \right] \sin(2kx) \mathbf{e}_y, \tag{1}$$

where $\langle E \rangle$ is the time averaged acoustic energy density, ω the angular frequency, V the particle volume, k the wavenumber, $\alpha = \rho_{\mathrm{p}}/\rho_o$ and $\beta = c_{\mathrm{p}}/c_o$, where $\rho_{\mathrm{p}(o)}$ is the particle (fluid) density and $c_{\mathrm{p}(o)}$ the speed of sound in the particle (fluid). In the

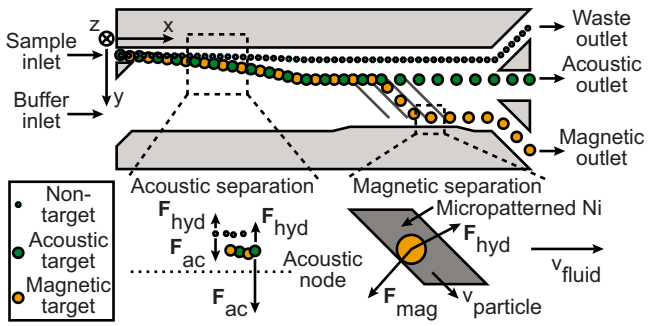

FIG. 1. (Color online) Overview of the IAMS device separation principle. The target and nontarget particles are introduced at the sample inlet alongside a buffer stream. Next, both acoustic and magnetic target particles are acoustically separated. The target particles are then magnetically separated by a series of microfabricated ferromagnetic structures. As a result, the acoustic and magnetic targets are eluted through two independent outlets.

a)Electronic addresses: tsoh@engineering.ucsb.edu and tsoh@engr.ucsb.edu.

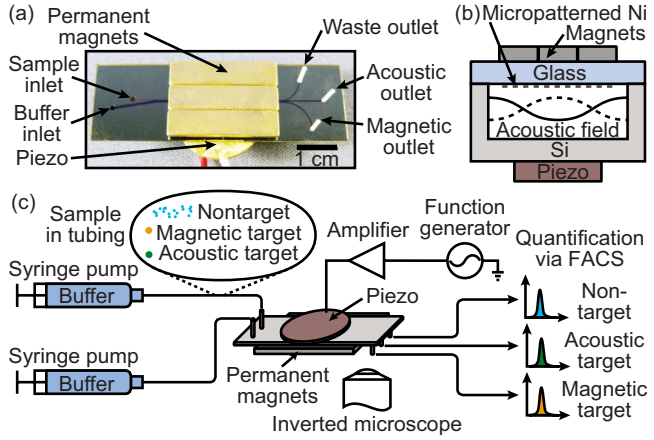

FIG. 2. (Color online) (a) Photograph of the assembled device, showing the acoustic and magnetic components and fluidic connections. (b) Cross-sectional schematic of the device, showing the relative locations of the magnets, micropatterned Ni and piezo, and the orientation of the acoustic field. (c) Schematic of the experimental setup. The sample containing acoustic target, magnetic target, and nontarget particles is loaded into inlet tubing and introduced alongside buffer solution into the IAMS device via dual programmable syringe pumps (PhD 2000, Harvard Apparatus, Holliston, MA). The microfabricated ferromagnetic structures within the device are magnetized by three neodymium iron boron permanent magnets. Acoustic resonances are excited by a single piezotransducer that is attached onto the back of the chip and driven by a function generator (33120A, Hewlett Packard, Palo Alto, CA) and custom-built amplifier based on an LT1210 op-amp (Linear Technology, Milpitas, CA). The separation process is observed via an inverted fluorescence microscope for monitoring during separation. The purities of the eluted fractions are analyzed via flow cytometry (FACSAria, BD Biosciences, San Jose, CA).

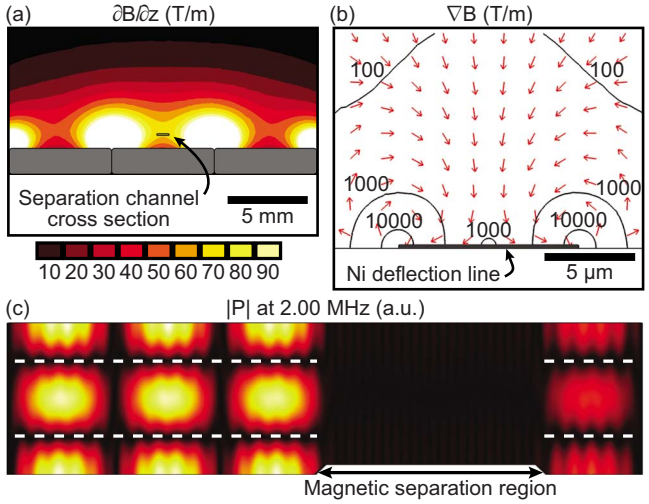

FIG. 3. (Color online) Simulation of acoustic and magnetic fields within the IAMS device (COMSOL Multiphysics, Comsol Inc., Los Angeles, CA). (a) Simulation of the long-range magnetic field from the external magnets shows that $\partial B/\partial z \approx 70$ T/m within the cross-section of the device. (b) Simulation of the short-range magnetic field due to a microfabricated Ni element. Contours show magnetic field gradient magnitude, arrows show gradient direction. (c) The acoustic resonance is locally disrupted by modulating the width of the microchannel. Longitudinal acoustic modes are indicated by the dashed lines.

acoustic separation region of the device (width 750 μm), two acoustic nodes exist at positions $y=187.5$ μm (node 1) and $y=562.5$ μm (node 2) at the operation frequency of 2.00 MHz. Thus, all particles are attracted toward node 1, which is nearer to the sample inlet. Because inertial effects are negligible at the low Reynolds number ($\mathrm{Re}_{\mathrm{IAMS}} \approx 10$) within our system, the acoustic radiation force $\langle \mathbf{F}_{\mathrm{ac}} \rangle$ acting on a particle is always counterbalanced by the Stokes hydrodynamic drag force $\mathbf{F}_{\mathrm{hyd}}=6\pi\eta a v_y \mathbf{e}_y$, where η is the fluid viscosity and a is the particle radius. Thus, the instantaneous transverse particle velocity may be expressed as $v_y(y)=\langle \mathbf{F}_{\mathrm{ac}} \rangle / 6\pi\eta a$. Using this relationship, we note large differences in the relative separation velocities between the target and nontarget particles, enabling efficient separation; the ratio of velocities between the acoustic target and nontarget was $v_{y,\mathrm{target}}/v_{y,\mathrm{nontarget}}=12.5$ to 25, and that between the magnetic target and nontarget ranged from $v_{y,\mathrm{target}}/v_{y,\mathrm{nontarget}}=17.5$ to 35, allowing for effective separation.

After nontarget particle depletion, the remaining particles are sorted in the magnetic separation region, where acoustic and magnetic targets get purified into independent outlets. The magnetic separation was performed as previously described by Adams *et al.*,[13] Inglis *et al.*,[14] and Smistrup *et al.*[17] Briefly, a set of three external NeFeB permanent magnets are used to create long-range magnetic field gradients that serve to attract all magnetic particles toward the bottom plane of the IAMS device, where large, short-range magnetic gradients are generated by microfabricated ferromagnetic structures.[13,17] We estimate the maximum time for the long-range force to move the particles to the bottom plane of the device as

$$\tau_s^{\max} \approx \frac{h}{v_z} = \frac{6\pi\eta a h}{m\left(\frac{\partial B}{\partial z}\right) + Vg(\rho_{\mathrm{p}} - \rho_o)}, \tag{2}$$

where h is the channel height and B is the magnetic field. In our device, using calculated values of the long-range magnetic field [Fig. 3(a)], we estimate $\tau_s^{\max}$ to be of order 40 ms, which is significantly shorter than the average particle residence time in the separation channel ($\tau \approx 400$ ms). This ensures that all magnetic particles reach the device bottom and are subsequently subject to short-range magnetic field gradients of order $\approx 10^3$ T/m within ≈ 5 μm of the ferromagnetic structures [Fig. 3(b)]. As described previously,[13] separation of magnetic targets from acoustic targets is achieved by balancing the magnetic force $\mathbf{F}_{\mathrm{mag}}$ and the hydrodynamic drag force $\mathbf{F}_{\mathrm{hyd}}$. Due to the fact that the Ni lines are oriented at an angle of 5° to the fluid flow, magnetic particles are selectively deflected and directed into the magnetic outlet if $F_{\mathrm{mag},\perp} > F_{\mathrm{hyd},\perp}$ (Fig. 1, inset right), whereas acoustic targets experience no magnetic force, and thus pass undeflected to eluted via the acoustic outlet.

Multiple design features of the IAMS device help enable high purity multitarget separation. First, the Ni patterns are not fully extended toward the separation channel edge (i.e., $y=0$) but begin at position $y=157.5$ μm. This ensures that the magnetically labeled targets are subject to both acoustic and magnetic forces, and must respond to both in order to reach the magnetic outlet. Second, to reduce the acoustic radiation force during magnetic separation, we have disrupted the acoustic resonance in the magnetic separation area by locally varying the width of the microchannel.[18] The resonance frequency in the channel is approximately $f \approx c_o n_y / 2W$, and so a local width reduction of 50 μm in the magnetic separation region of our device increases the local resonance frequency by 7%. Numerical simulations revealed that such perturbations are sufficient to completely exclude

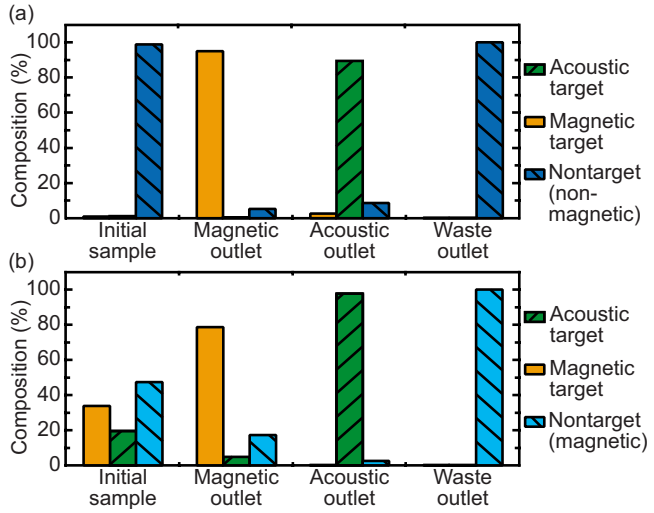

FIG. 4. (Color online) (a) Separation of a mixture of acoustic target, magnetic target, and nonmagnetic nontarget, showing enrichment to very high purity starting from rare (<1%) amount of each target. (b) Separation of a mixture of acoustic target, magnetic target, and magnetic nontarget, demonstrating that particles entering the magnetic outlet must respond to a combination of both separation forces.

acoustic resonances within the magnetic separation region [Fig. 3(c)]. Experimentally, we observed some resonance, which may be due to resonance-broadening effects in the device.[18]

We tested the performance of the IAMS device using 5 μm diameter fluorescent green polystyrene particles as acoustic targets (G0500, Duke Scientific, Palo Alto, CA), 4.5 μm diameter magnetic microspheres as magnetic targets (M-450, Invitrogen, Carlsbad, CA), and 1 μm diameter blue fluorescent polystyrene particles as nontargets (B0100, Duke Scientific). Magnetic targets were conjugated streptavidin (SA) (New England Biolabs, Ipswich, MA) and subsequently labeled with SA-phycoerythrin (Invitrogen, Carlsbad, CA) to enable simple analysis via flow cytometry. We designed our test to replicate rare target separation from a large nontarget background, starting with a mixture of 0.9% acoustic target, 0.7% magnetic target, and 98.4% nontarget particles. Sample and buffer were introduced into the device at throughputs of 0.5 ml/hr (10^8 particles/hr) and 20 ml/hr, respectively. The piezo was driven at 2.00 MHz and 26 V_{pp}. As shown in Fig. 4(a), the IAMS device achieved very high-purity separation; output at the magnetic outlet consisted of 94.8% magnetic target, 0.2% acoustic target, and 5.0% nontarget. The fraction at the acoustic outlet contained 89.2% acoustic target and 2.4% magnetic target at 8.4% nontarget. 91% of all target particles were removed from the waste stream, demonstrating sufficient target recovery.

We then applied more stringent separation conditions by using magnetic nontarget particles (MyOne Streptavidin, Invitrogen), such that particles are sorted based on both size and magnetic content. We sorted a sample containing 19% acoustic target, 34% magnetic target, and 47% nontarget under the same conditions described above. After a single pass, the purity obtained at the acoustic outlet was 97%, while the purity at the magnetic outlet was 78% [Fig. 4(b)]. Furthermore, 99.6% of all target particles were separated from the nontargets, confirming that particles entering the magnetic outlet are responding appropriately to the combination of separation forces.

In conclusion, we have demonstrated the integration of acoustic and magnetic separation in a monolithic device. Microfabrication of channels and ferromagnetic structures allowed precise control of acoustic resonances, fluidic drag, and magnetic forces, enabling high-purity particle separation at high throughput ($\approx 10^8$ particles/hr). We believe that our integrated architecture could be suitable for a wide range of biological applications. Magnetic deflection has been previously applied toward targets ranging in size from bacteria to mammalian cells, via labeling with either magnetic nano or microparticles.[13,14] Furthermore, because $F_{ac} \propto V/\lambda$, for microscale systems, particle sizes ranging from one up to tens of micrometers generate sufficient acoustic force to be separable. To achieve acoustic separation of smaller bacteria and viruses, particles displaying specific surface markers could be used as labeling agents. Finally, in order to ensure that neither separation force dominates, proper adjustment of the relative magnitudes of each could be accomplished through changes to the piezo driving voltage and the external magnetic field strength.

We are grateful for the financial support from ONR (Grant No. ONR N001480810469), NIH (Grant Nos. NIH 1R21EB009518 and NIH 1R01EB009764), ARO Institute for Collaborative Biotechnologies (ICB), and Armed Forces Institute for Regenerative Medicine (AFIRM). We thank Unyoung Kim for help with flow cytometry, and B. Scott Ferguson for helpful discussions. Microfabrication was carried out in the Nanofabrication Facility at UC Santa Barbara.

[1]C. E. Sims and N. L. Allbritton, Lab Chip **7**, 423 (2007).
[2]J. El-Ali, P. K. Sorger, and K. F. Jensen, Nature (London) **442**, 403 (2006).
[3]H. M. Shapiro, *Practical Flow Cytometry*, 4th ed. (Wiley, Hoboken, NJ, 2003).
[4]S. F. Ibrahim and G. van den Engh, Curr. Opin. Biotechnol. **14**, 5 (2003).
[5]J. Seidl, R. Knuechel, and L. A. Kunz-Schughart, Cytometry **36**, 102 (1999).
[6]S. Miltenyi, W. Muller, W. Weichel, and A. Radbruch, Cytometry **11**, 231 (1990).
[7]I. Safarik and M. Safarikova, J. Chromatogr., B: Biomed. Sci. Appl. **722**, 33 (1999).
[8]M. Wiklund, C. Gunther, R. Lemor, M. Jager, G. Fuhr, and H. M. Hertz, Lab Chip **6**, 1537 (2006).
[9]S. K. Ravula, D. W. Branch, C. D. James, R. J. Townsend, M. Hill, G. Kaduchak, M. Ward, and I. Brener, Sens. Actuators B **130**, 645 (2008).
[10]U. Kim and H. T. Soh, Lab Chip **9**, 2313 (2009).
[11]F. Petersson, L. Aberg, A. Sward-Nilsson, and T. Laurell, Anal. Chem. **79**, 5117 (2007).
[12]N. Pamme and C. Wilhelm, Lab Chip **6**, 974 (2006).
[13]J. D. Adams, U. Kim, and H. T. Soh, Proc. Natl. Acad. Sci. U.S.A. **105**, 18165 (2008).
[14]D. W. Inglis, R. Riehn, R. H. Austin, and J. C. Sturm, Appl. Phys. Lett. **85**, 5093 (2004).
[15]See EPAPS supplementary material at http://dx.doi.org/10.1063/1.3275577 for fabrication details.
[16]K. Yosioka and Y. Kawasima, Acustica **5**, 167 (1955).
[17]K. Smistrup, O. Hansen, H. Bruus, and M. F. Hansen, J. Magn. Magn. Mater. **293**, 597 (2005).
[18]O. Manneberg, S. M. Hagsater, J. Svennebring, H. M. Hertz, J. P. Kutter, H. Bruus, and M. Wiklund, Ultrasonics **49**, 112 (2009).